Ultrasonic Characterization of Surfaces and Interphases

Stanislav I. Rokhlin and Theodore E. Matikas

Introduction

Ultrasonic waves have been used extensively for material characterization and for sensing in material process control. The waves produce small-amplitude mechanical vibrations and, depending on the mode being used, may induce both longitudinal and shear stresses in the solid. Information on the structural properties of a substance can be obtained by measuring both the velocity and the attenuation of the ultrasonic wave. The phase velocity of the wave depends on the elastic constants and density of the body while attenuation depends on microstructure and crystalline defects.

In an *isotropic* solid medium, which has only two independent elastic moduli, there exist two elastic waves: the longitudinal and the shear. Three kinds of bulk elastic waves may propagate in an *anisotropic* solid: a quasilongitudinal and two quasitransverse waves, differing in polarization and velocity. To determine the set of elastic constants, one must measure the phase velocity in several different directions relative to the crystallographic axes.[1,2]

The attenuation of an ultrasonic wave is associated with absorption of elastic waves (inelastic effect) and the scattering of elastic waves by structural inhomogeneities.[1] Scattering may be the governing attenuation mechanism in polycrystalline, composite, and ceramic materials. As a result of scattering, elastic energy is lost by the prime ultrasonic beam in the form of a stochastically scattered field, which is gradually absorbed in the material. The latter is associated with conversion of elastic into thermal energy as a result of various inelastic effects termed internal friction.

The elastic moduli (and ultrasonic velocity) and elastic-wave attenuation are affected by the microstructure. If one knows the effect of microstructure on mechanical properties such as strength, ultrasonics could be used for nondestructive evaluation of the mechanical properties of the material.

While methods of ultrasonic characterization of materials in bulk are widely known in the material-science community, methods for characterization of thin surface and interphase layers are much more specialized and less developed. Here we will review some advances in this field.

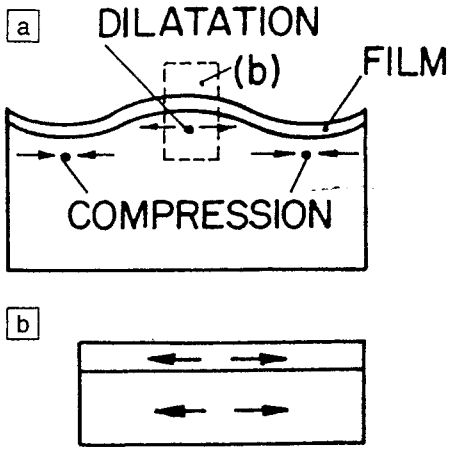

Figure 1. (a) Deformation of a surface of a solid body with coating. (b) Longitudinal strain of a surface film on propagation of a Rayleigh wave.

Characterization of Thin Films Using Elastic Surface Waves

Surface waves are often used to measure the properties of a very thin layer of material, the thickness of which is much smaller than the thickness of the substrates. Since the mechanical properties of the film-substrate system are controlled not only by the bulk properties of the film but also to a significant degree by the adhesion of the film to the substrate, the properties of the film-substrate interphase are also of prime interest.

As shown by Rayleigh, an elastic surface wave may propagate along the surface of a solid body.[2,3] The elastic energy of surface waves decays nearly exponentially from the surface and is localized in a subsurface layer with thickness of the order of wavelength λ. At a depth of the order of λ, there is virtually no transport of elastic energy.

The presence of a thin film on the substrate surface changes the surface stiffness and also loads the surface. Figure 1 shows schematically that a thin film, whose thickness is much less than a wavelength, is subjected to a compression-tension strain in the course of surface-wave propagation. The strain arising in the film is similar to the strains in a thin plate upon propagation of a longitudinal plate mode. In this case, the velocity of the surface wave depends not only on the substrate properties but on the stiffness $E_0/(1-\nu_0^2)$ and the density ρ_0 of the film. (E_0 is Young's modulus, and ν_0 is the film Poisson ratio.)

Measurements of the surface-wave velocity can yield information on the coating properties and the condition of the bond between the coating and the substrate. Three methods are possible: (a) direct measurement of the velocity and attenuation of the surface wave, (b) the Rayleigh angle method, and (c) acoustic microscopy.

Direct Measurement of the Velocity and Attenuation of Surface Acoustic Waves

There are no standard techniques or equipment for thin-film characterization using surface acoustic waves (SAW). However such measurements have been performed for a long time in different laboratories. Measurement of SAW attenuation[4,5] has been used for the study of properties of thin films as a function of magnetic field or temperature. Measurements of the velocity and attenuation of SAW during deposition of thin films were also described.[6,7]

A noncontact laser ultrasonic method could be used for this purpose, as shown

in Figure 2.[8,9] A pulsed laser generates thermoelastic stresses on the specimen surface, which leads to excitation of a surface wave. A laser interferometer can be used as a receiver. The noncontact nature of the technique is important in the case of ceramic coatings,[10,11] some of which can be damaged by contamination with ultrasonic couplants. In addition the method can be utilized on hot surfaces and has a potential for utilization during manufacturing (e.g., for measurement of deposition of a coating on a substrate). Examples of thin diamond-film measurements are given in Reference 12. A different technique employing interdigital transducers has been utilized in Reference 13 for characterization of the diffusion reaction in Au-Al thin-film diffusion couples. These techniques can be utilized in the 10–100-MHz frequency range and used for film characterization in the 0.1–1-μm thickness range.

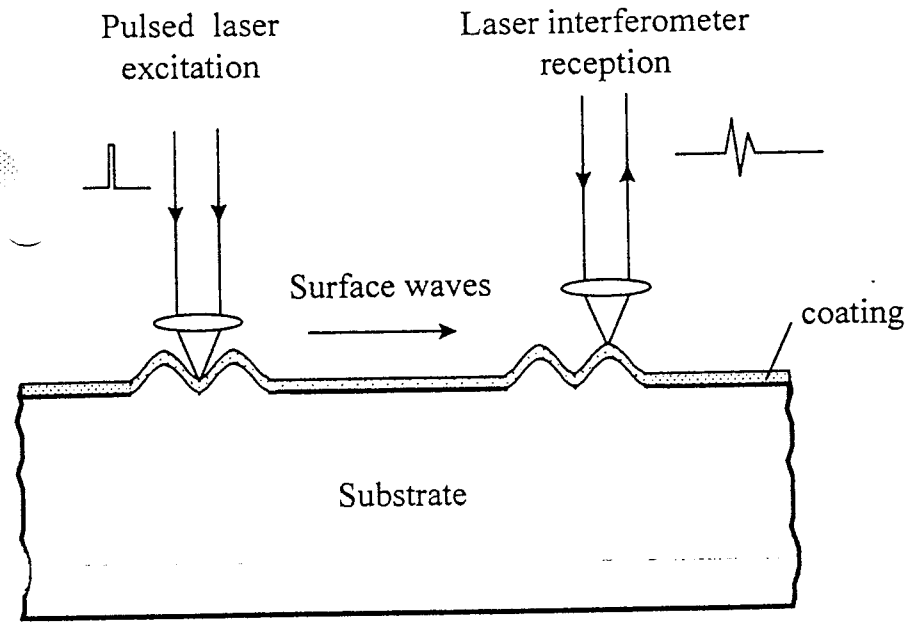

Figure 2. Schematic of surface-wave generation by a laser.

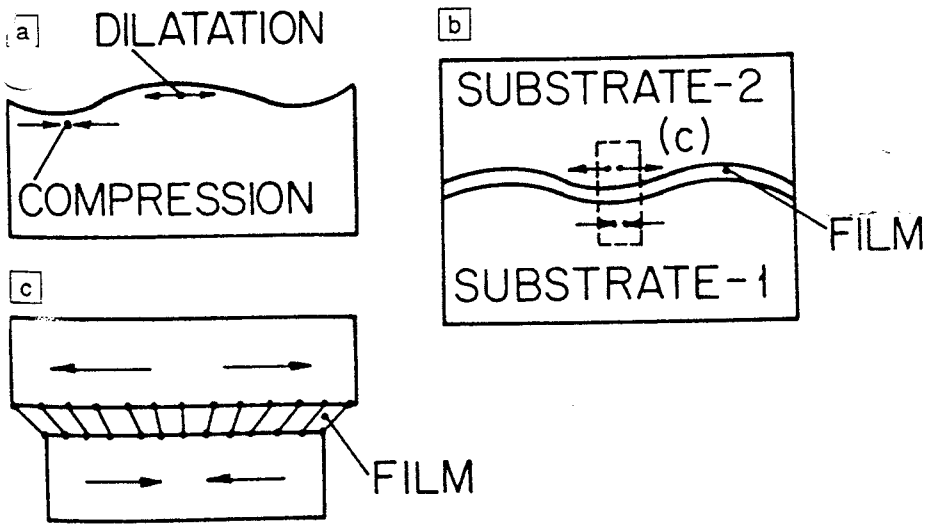

Figure 3. (a) Deformation of the surface of a solid body upon propagation of a Rayleigh wave. (b) Deformation of an interphase film upon propagation of an interface wave. The thickness of the interphase film is much smaller than the interface wavelength. (c) Shear strain of the interphase film. The figure corresponds, on a magnified scale, to element (c) singled out in Figure 3b.

Rayleigh Angle Method and Acoustic Microscopy

When an elastic half space is loaded by a fluid, a Rayleigh-type surface wave can propagate on a solid-liquid interface. The surface-wave velocity V_r is usually higher than the velocity of the acoustic wave in a fluid (e.g., V_r in metals is about 3 km/s whereas the velocity of sound V_0 in water is about 1.5 km/s). This results in radiation (leakage) of elastic energy of the surface wave to the liquid. Therefore such a wave is termed a leaky surface wave. The radiation angle of the nonhomogeneous leaky wave is obtained from Snell's law. Interaction of the incident ultrasonic beam with the solid at the Rayleigh angle can be utilized for surface-wave-velocity measurements.

The velocity and attenuation of a surface wave can be determined with sufficient accuracy from the measured amplitude and phase of the reflected beam.[14] An analysis of the method for determination of elastic properties of thin layers was carried out by Chimenti, Nayfeh, and Buter.[15] Application to thermal-shock damage characterization in ceramics has been described in Reference 16.

Acoustic microscopy is a relatively new tool for ultrasonic characterization of near surface properties of materials and is discussed in detail in the article by Briggs and Kolosov in this issue of *MRS Bulletin*. Acoustic microscopy operates in a C-scan mode, providing an ultrasonic reflection image in the plane parallel to a sample surface. The major difference in image formation between the acoustic microscope and a conventional focus probe C-scan is that the contrast in the acoustic microscope is formed by interference between the wave reflected from the material surface and the leaky surface wave generated and received by the acoustic lens, instead of consideration of the reflected wave only. The interference pattern representing the variation of the interference signal amplitude with distance z between the sample and the lens is called the $V(z)$ curve.

For anisotropic materials, the angle dependence of surface-wave velocity is required. This can be obtained using a line acoustic microscope with a cylindrical lens. Systematic application of line

acoustic microscopy for anisotropic materials and thin-film characterization is described by Achenbach et al.[17] The method is based on collecting $V(z)$ curves at different lens orientations, and the elastic constants of the material are recovered from surface-wave-velocity V_r measurements as a function of angle.

The $V(z)$ curve method applied in acoustic microscopy for V_r measurements is time-consuming. Time-resolved acoustic microscopy uses a short pulse so that specular reflection and leaky surface-wave signals are resolved in the time domain.[18,19] In this case, the velocity measurement is reduced to time-delay measurement. This technique provides a fast and precise option for surface-wave-velocity measurements. Johnson et al.[19] used this technique for diamond-film characterization. The film thicknesses were 100–500 μm, and the frequency range was about 50 MHz.

Interphase Layer Properties Measurement Using Elastic Interface Waves

In the previous section, the application of surface waves was described for surface film characterization. The velocity of the surface wave could be used to measure the longitudinal stiffness $E/(1-\nu^2)$ of the thin films. For elastic-modulus measurements of thin interphase films, elastic interface waves can be utilized and the shear modulus determined.

The term "elastic interface waves" is used to denote waves propagating along the interface between two media and localizing the energy in a band with a width of the order of the wavelength. An interface wave of a special type, termed the Stonley wave, may propagate along the interface between two elastic half spaces in welded contact with one another. The velocity of the Stonley wave should be lower than the velocities of the shear waves in the half spaces. This condition imposes rigid limitations on the ratio of the elastic moduli and densities[2] of the possible pairs of half spaces. In the general case, the Stonley wave is a leaky wave, and its energy is radiated in the form of a shear-wave velocity (slow half space).

The gradual transformation of a Rayleigh wave into a Stonley wave due to the strong pressing together of two solids was observed experimentally[20,21] and discussed theoretically within the framework of a phenomenological model[22,23] of a loosely bonded interface. This can be used for the evaluation of dry contact between two solids.

A more general case of interface waves exists in a system of two half spaces separated by a viscoelastic layer.[24,25] The interface wave is localized if the shear modulus μ_0 of the layer is smaller than the shear modulus of the half spaces. Such a model satisfactorily approximates an adhesively bonded specimen, provided that the adhesive thickness is much smaller than that of the substrates. The deformation of a thin solid interphase film by the interface wave is illustrated schematically in Figures 3a and 3b where the deformation of an interphase layer, the thickness of which is much smaller than the wavelength, is shown. Due to antisymmetry of motion, the interphase layer is subjected to shear strain (Figure 3c). To excite an interface wave, one can use mode conversion from a surface wave[24] or excite it from the edge of the sample.[26]

One can estimate the viscoelastic properties of the interphase layer by measuring the velocity and attenuation of the interface wave. The complex shear modulus μ_0 of an interface wave is related by a simple expression to the interface-wave velocity V_i for thin isotropic[24] or anisotropic[27] layers.

Characterization of Imperfect Interphases: Modeling

It is well-established that the mechanical integrity of interphases plays a major role in determining the serviceability of structures and their components. Examples include but are not limited to solid-state bonds, adhesive joints, and coated and laminated materials. New advanced materials, such as high-temperature ceramic- and metal-matrix composites, are designed with specially tailored interphases to increase material fracture resistance and accommodate residual stresses. Despite great attention to quality in the development of manufacturing processes, interphases are still the weakest link in the mechanical performance of components.

The challenge is to evaluate imperfect interphases with microdefects, microstructural changes, or areas in tight mechanical contact without chemical or metallurgical bonds. The difficulty is to delineate and quantitatively describe such interphases by using nondestructive evaluation. Another challenge is to relate such measurements to mechanical properties. Such a relationship comes from the dependence of interphasial strength on interphase microstructure and the existence and morphology of microdefects. If one can determine such interphasial characteristics nondestructively and can determine a relation between microstructure and mechanical properties, one can obtain a nondestructive prediction of strength and life expectancy.

When two materials are bonded together by solid-state or other processes, different types of imperfections may form in the bond line. Plane disbonds usually have negligible thickness and can be considered cracks. Also volumetric flaws such as voids or microinclusions may appear. It is important to discern these types of defects since pla-

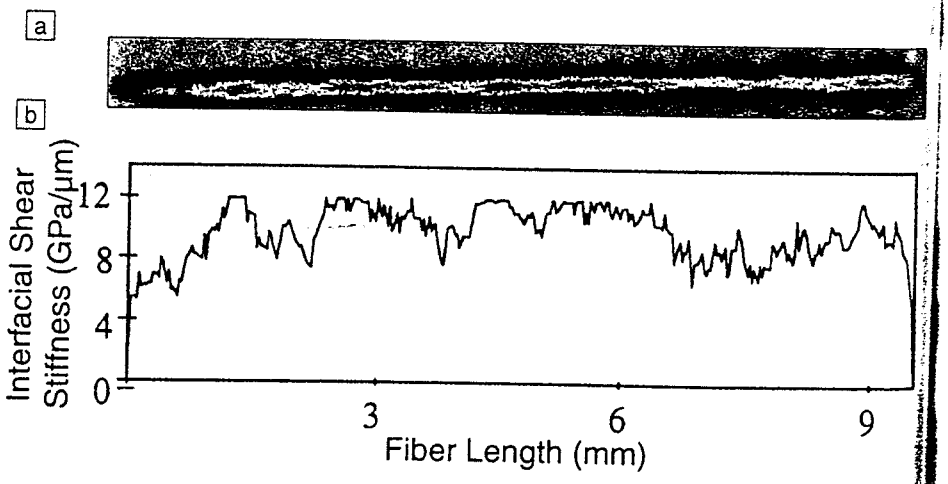

Figure 4. (a) Ultrasonic shear back-reflectivity image of a 142-μm-diameter SiC fiber (SCS-6) embedded in a titanium matrix (Ti-6Al-4V). The variation in colors along the fiber indicates variation in the modulus of the interphase. (b) The corresponding values of shear stiffness along the fiber obtained using the ultrasonic-reflectivity measurements and the model in Reference 47. The average shear stiffness of the Ti-6Al-4V/SCS-6 interphase was about 9 GPa/μm.

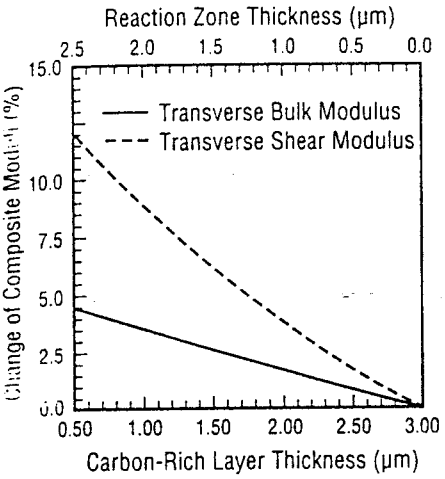

Figure 5. Normalized composite transverse moduli versus the thickness of the carbon-rich layer in a Ti-based intermetallic-matrix composite (SCS-6/Ti-24Al-11Nb). The calculations simulate the changes of the composite moduli during processing when the carbon-rich layer thickness decreases from 3 to 0.5 μm and the reaction zone grows from 0 to 2.5 μm. (The total thickness is constant [3 μm].) The composite modulus change is primarily due to decrease in the carbon-rich layer thickness.

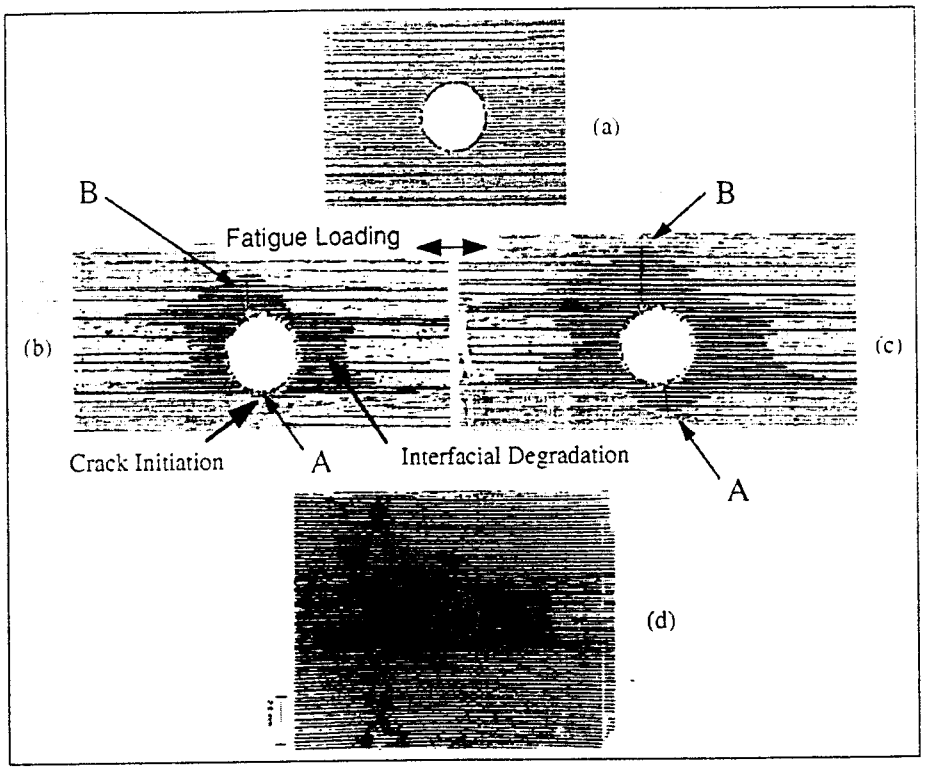

Figure 6. Ultrasonic images of a bi-directional [0/90]8 TiMetal/SCS-6 titanium matrix composite with circular notch configuration. (a) Image prior to mechanical testing. (b) Image following 10^5 cycles isothermal fatigue at 650°C for 43 hours. (c) Image following an additional 10^5 cycles fatigue at 650°C for 27 hours. (d) Metallography of the sample.

nar flaws lead to stress concentration and significant strength reduction of the interface. Ultrasonic waves may serve as a powerful tool for interphase characterization since they are able to penetrate different solids and are sensitive to material inhomogeneities. Modeling of elastic-wave interaction with an interface (mechanistic representation of the interphase region) plays an important role in interpretations of the ultrasonic interface signature.

To describe ultrasonic-wave interaction with a cracked interface, a simple spring boundary-conditions model was proposed as follows:[28]

$$\sigma_{zz}^{+} = \sigma_{zz}^{-} = K_l(u_z^{-} - u_z^{+})$$
$$\sigma_{xx}^{+} = \sigma_{xx}^{-} = K_t(u_x^{-} - u_x^{+}) \quad (1)$$

where z is perpendicular and x is parallel to the interface, σ^{+} and u^{+} are the stress and displacement on the upper side of the interface, and σ^{-} and u^{-} are the stress and displacement on the bottom. The quantities K_l and K_t are longitudinal (l) and transverse (t) distributed spring constants. Using the available static fracture mechanics solution for a cracked interface, K_l and K_t were defined[28] so that the overall compliance of the cracked interface is equal to that with the equivalent springs. To account for interface inertia, mass terms can be included in the boundary conditions (Equation 1).[28,29] When the interphase includes volumetric imperfections such as voids, inclusions, or imperfections formed by rough surfaces, it is natural to consider the interphase as a nonhomogeneous multiphase (composite) layer.[30] The validity of this model was established[30] by comparing the coefficient of reflection from the composite layer to the numerical solution of the diffraction problem[31] for the array of voids. If the wavelength λ_0 of the ultrasonic wave in the interphase medium is greater than the layer thickness h, the exact wave solution in the layer may be expanded asymptotically to describe the equivalent boundary condition at the interface[32-34] for isotropic or anisotropic layers. Spring boundary conditions (Equation 1) can be obtained by simplifications of this model. Mathematically it is much simpler to analyze wave phenomena using the asymptotic boundary conditions than the exact solution since there is no need to describe the wave behavior inside the interphasial layer.

Wave interaction with an interface as a scattering process was considered in Reference 35 using both independent-scattering and multiple-scattering[36] theories and gives good results in comparison with experiment.[29,36] To use the model, one should know the mean-scattering far-field amplitude from a single scatterer—a function of the frequency, size, shape, and other properties of the inhomogeneity. This may complicate inversion of the ultrasonic measurements.

As we just discussed, different models can be used successfully to treat ultrasonic-wave interaction with imperfect interfaces. The goal of ultrasonic characterization is to characterize interface imperfections based on the ultrasonic signature. The models may help in selecting different experimental approaches to find the model parameters and the imperfection characteristics. It is clear that unique inversion of ultrasonic data to

find imperfection parameters is a complicated task. An important question is how to discriminate between the planar (cracklike) or volumetric (voidlike) interphasial flows. The interphasial stiffness ratio K_t/K_l was suggested as such a classifier.[37-39] As follows from the spring model[28] for interfaces with planar circular cracks (disbonds), the ratio is unity ($K_t \approx K_l$). Equality of the transverse and longitudinal (normal) stiffness due to cracks occurs not only for interphasial cracks but also for a cracked bulk solid.[40] As follows from the composite model,[30] for interphases with an array of volumetric flaws such as pores, the stiffness ratio becomes $K_t/K_l = C_{55}/C_{33}$ (where C_{ij} are elastic constants), which must be smaller than unity. For an isotropic interphasial layer, $K_t/K_l \approx 0.3$. Thus the ratio K_t/K_l is a useful parameter to distinguish planar disbonds from volumetric interphasial flaws. It was demonstrated in Reference 41 that the stiffness ratio also can be used to determine the type of interphasial damage between fibers and matrices in composites.

Ultrasonic Characterization of Interphases in Composites

It is well-known that the fiber-matrix interphase plays an important role in determining composite performance. The interphase not only allows load transfer between fibers and matrix but also provides chemical and thermal compatibility between the constituents. In metal- and intermetallic-matrix composites, special interphasial reaction barrier coatings and compliant coatings are introduced to improve chemical and thermal compatibility. In ceramic-matrix composites, the interphase is designed to provide frictional sliding contact between fiber and matrix to prevent fiber fracture due to matrix cracking. The interphase microstructure and its reaction with other composite constituents have received increasing attention. Despite great efforts in the development of special fiber coatings to tailor the interphase, the mechanical properties of the interphase remain difficult to measure and interpret. The complexity of such interphases will become even greater if the properties are altered during manufacturing or in service by chemical reaction between the constituents, or if micromechanical defects occur.

Several ultrasonic techniques could be utilized for the interphase characterization in higher temperature ceramic-matrix and metal-matrix composites. The interphase is considered to be a thin multilayered coating between the fiber and matrix. One technique measures the frequency dependence of the ultrasonic attenuation in the composite.[42,43] By modeling the scattering of ultrasonic waves from the fiber-matrix interphase, the attenuation data can be related to the interphase elastic properties by accounting for scattering losses from the fibers. The second approach is based on measurements of ultrasonic phase velocities to find the composite elastic moduli, which are used to determine the interphase moduli via micromechanical analysis.[44,45] Another potential ultrasonic method is based on the wave velocity and attenuation measurements along the fiber length in the composite.[46]

An ultrasonic shear-wave-back-reflectivity (SBR) technique[47,48] can provide nondestructive characterization of local fiber-matrix-interface shear elastic properties. This method is based on propagating shear ultrasonic waves in the material and monitoring the back-reflected waves at the interphase. A micromechanics model relates the back-reflected shear-wave ultrasonic signal to the local shear stiffness of the interphase, which is defined as the ratio of the interphase shear modulus and the thickness of the interphase at a particular location along the fiber. The technique provides both imaging and quantitative information about the variations of interphase elastic property along the fibers. Figure 4 shows an example of interphase characterization for a SiC (SCS-6) fiber embedded in a metal (Ti-6Al-4V) matrix using the shear-wave reflectivity technique. Variations in ultrasonic reflectivity along the fiber, shown in Figure 4a, indicate variations in the modulus of the interphase. Using the model in Reference 47, these variations can be quantified (Figure 4b). This technique has been applied to control composite formation[49] such as localized consolidation[50] and matrix microstructure.[51] Also it has been used to detect fiber fracture[52] as well as to monitor interphase degradation in both metal-matrix and ceramic-matrix composites.[53,54]

The method for interphase characterization based on ultrasonic attenuation measurement is applicable for composites with large-diameter fibers, as in the case of SiC fiber composites, where scattering by the matrix microstructure

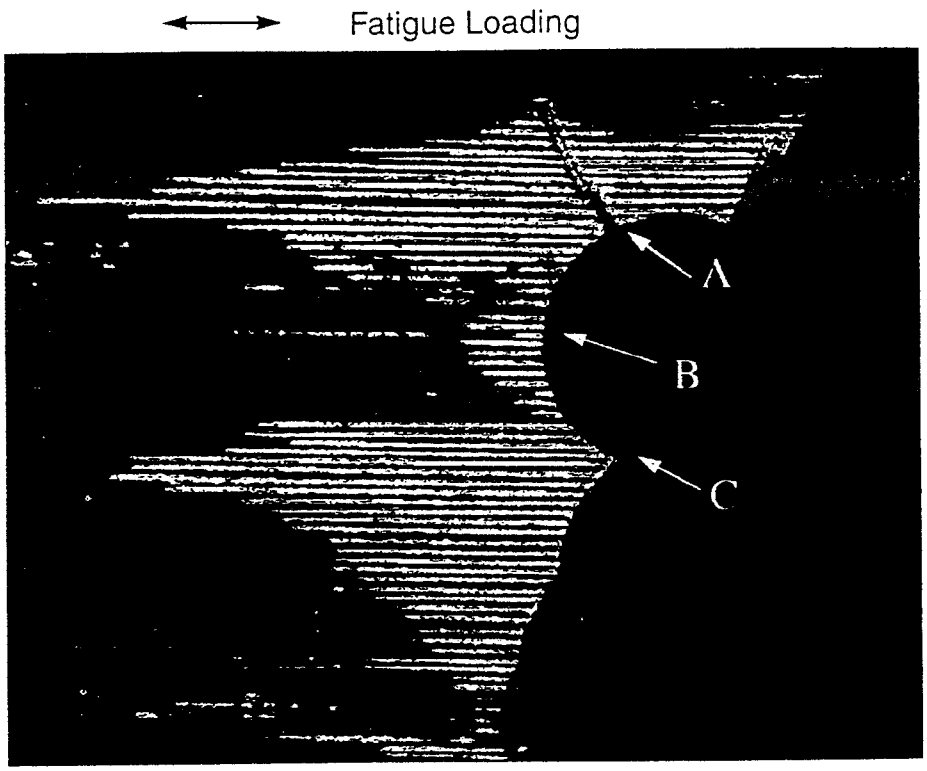

Figure 7. Ultrasonic image of unidirectional TiMetal/SCS-6 composite after undergoing isothermal fatigue for 1.82 × 10^5 cycles at 650°C. (A: matrix crack. B: interfacial degradation due to compressive stresses. C: interfacial degradation due to tensile stresses.)

(porosity, grains, etc.) is negligible compared to that from fibers. In this case, the fiber-matrix interphase condition affects greatly the wave propagation in composites. By measuring the frequency dependency of the wave attenuation, one can infer information about the fiber-matrix interphase.[55,56] Scattering models[43,46,55] were developed to establish the quantitative relationship between wave attenuation in the composite and the fiber-matrix interphase conditions. It was shown that wave attenuation and velocity measured using the amplitude and phase spectra of the transmitted signals are in agreement with the scattering model prediction and could be used for damaged interphase characterization.

The use of ultrasonic phase velocity data to characterize the fiber-matrix interphase has been implemented using various micromechanical schemes.[45,46,57–60] The ultrasonic phase velocities in composites are first measured and used to determine the composite moduli, which are then used to calculate the interphasial moduli via inversion of micromechanical models. The relation between the elastic constants C_{ij} of an anisotropic medium and the phase velocities of ultrasonic waves in the medium is given by the Christoffel equation.[1,2] To determine the composite elastic constants from the ultrasonic-phase-velocity measurements, one inverts the Christoffel equation applying a nonlinear least-squares optimization technique.[61,62] It was shown[63,64] that the relative error in the elastic constants so determined is similar to that in the velocity measurements, which is less than 1%.[64] When composite and constituent moduli are measured within 1% error, the determined interphasial moduli have about 5% error.[59] The success of the inversion method depends on the sensitivity of the composite moduli to variation of the interphasial moduli. When the fiber is stiffer than the matrix and the interphase is a compliant layer, the composite moduli depend strongly on the interphasial moduli.

For composites reinforced with SiC (SCS-6) fibers, a multiphase microstructure must be considered due to the presence of the fiber core (carbon), shell (SiC), and carbon-rich coating. Different models have been developed for inversion with similar results. One approach[45,58] replaces the core-shell combination with a so-called "equivalent" fiber, simplifying the microstructure and using three-phase models for inversion. Another approach[57] utilizes finite-element analysis where the fiber core and shell are considered as different phases. More recently a multiphase-generalized-self-consistent model has been developed.[59] As a result, analytical expressions for the transverse shear moduli of composites with multiphase fibers have been obtained using transfer-matrix formulation[59] and spring approximation.[60] This development allows the interphasial moduli to be determined from inversion of the multiphase model without the use of finite-element analysis or the equivalent fiber concept.

To demonstrate the feasibility of monitoring the interphase microstructure during processing under long-term heat exposure, the change of the composite modulus resulting from the reaction-zone growth for an intermetallic-matrix composite[60] is shown in Figure 5. In the calculations, the moduli of the reaction zone are taken to be 25% above the matrix moduli. The moduli of the carbon-rich layer are assumed to be constant, and its thickness decreases from 3 to 0.5 μm. The reaction-zone thickness grows from 0 to 2.5 μm, as a result of chemical reaction between the matrix and the carbon-rich layer, at the expense of reduction of the carbon-rich layer thickness. The composite transverse shear modulus changes quite significantly due mainly to shrinkage of the carbon-rich layer. This method could be important for evaluating the effect of long-term high-temperature exposure in service.

The interphasial moduli obtained from ultrasonic velocity data are "effective" moduli that depend on the state of contact between the fiber coating and the adjoining fiber and matrix. For better contact, such as is the case of intermetallic-matrix composites, the effective prop-

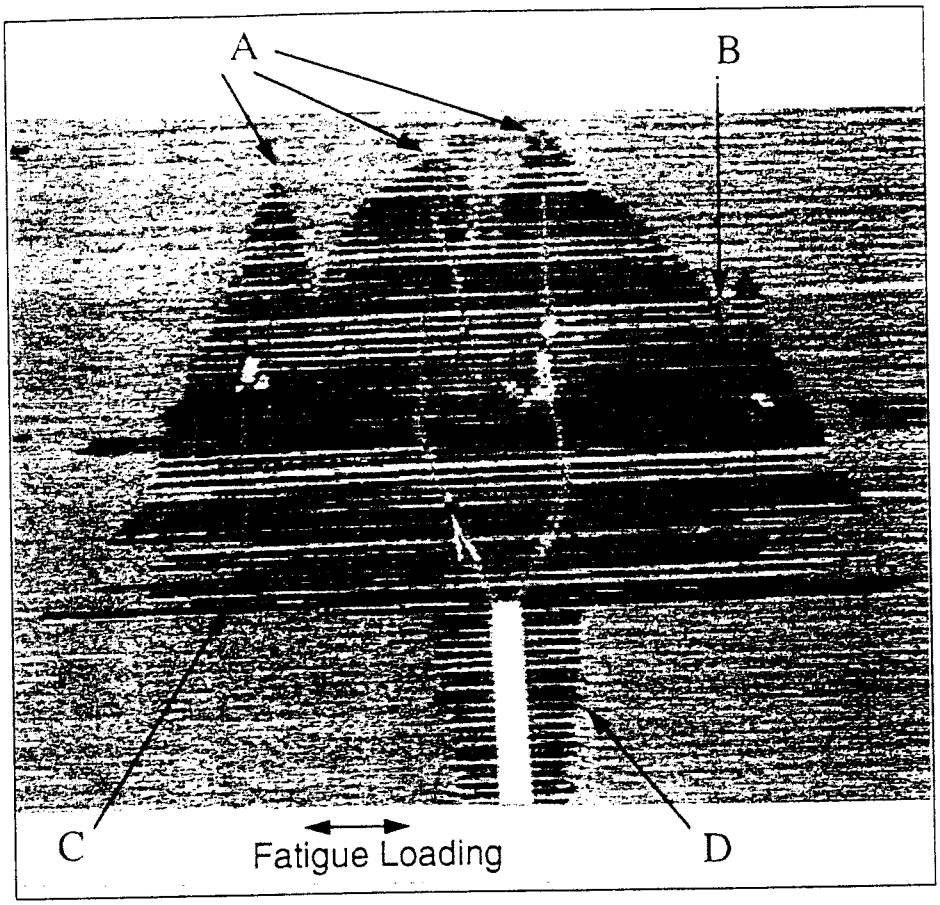

Figure 8. Ultrasonic image of TiMetal/SCS-6 composite with single-notch configuration following thermomechanical fatigue: load ratio R = 0.1 with maximum load P_{max} of 3.3 kN, 150–538°C; 36 days at 0.0056 Hz; out-of-phase. (A: high stress, high temperature, short duration. B: low-stress region between two cracks. C: high stress, high temperature, long duration. D: low stress, high temperature, long duration.)

erties are close to the actual properties of the interphasial layer while vanishing moduli correspond to complete fiber debonding from the matrix. Thus deviation of the measured interphasial moduli from the desired (designed) moduli may serve as a measure of the contact between the interphasial layer and the matrix, as in the case of ceramic-matrix composites.[55,58]

Application to Interphasial Damage Assessment in Composites

Oxidation damage is a major concern for ceramic-matrix composites and has been a critical area for composite development. Successful prevention of oxidation damage requires identification of dominant damage mechanisms. It is known[65] that one major damage mechanism is oxidation of the fiber-matrix interphases. The interphase characterization techniques described previously could be used to quantify the damage severity and identify the transition from the nonoxidized to the oxidized state.[66] The measured ultrasonic phase velocities are significantly reduced by the oxidation damage. The composite moduli calculated from the measured velocity data decrease as the oxidation exposure time increases.[67] The transition from the nonoxidized to the oxidized state can be quantified by determining the effective interphasial moduli for different exposure times. It was found that initial stages of interphase damage, when carbon coating/matrix separation occurs on the atomic scale, can be identified.[67]

Ultrasonic techniques have also been applied to assess environmental degradation of interphases in adhesive joints[68] and interphasial damage in titanium matrix composites due to mechanical fatigue[42] and thermomechanical fatigue at elevated temperatures.[69-71]

To demonstrate the utility of ultrasonic characterization for interphase damage assessment, Figure 6 shows ultrasonic images of a titanium matrix composite (B21S/SCS-6)[69] with a [0/90]8 cross-ply lay-up of fibers and a circular notch subjected to isothermal fatigue at elevated temperature. The fatigue experiment was periodically interrupted, and the first ply of fibers was imaged using ultrasonic surface-wave imaging. The pretesting image (Figure 6a) shows no interphasial damage prior to testing. The specimen was then isothermally fatigued at 650°C, and the test was stopped after 10^5 cycles for imaging (Figure 6b). The damage (as indicated by the high contrast regions in Figure 6b) originates at the top and bottom of the hole and proceeds away from the hole along the fibers. A crack was initiated at the bottom of the hole (as indicated by arrow A in Figure 6b) and then propagated as shown in Figure 6c, which shows the ultrasonic image after an additional 10^5 cycles. By comparing Figures 6b and 6c, the propagation of damage in the material can be observed—both microcracking growth and interphase oxidation. To substantiate the ultrasonic imaging, metallography (Figure 6d) was performed after removal of the outer matrix layer. This image corresponds to the same stage of damage as the ultrasonic image in Figure 6c. Comparison between Figures 6c and 6d demonstrates significant advantage of ultrasonic imaging for characterization of early stages of interphase degradation that occurred only after development of cracks A and B (Figure 6c). However good correlation of interphasial oxidation between ultrasonic and metallographic images was observed for fibers with edges exposed directly to the oxygen (fibers left and right of the hole). This interpretation of oxidation damage development observed by ultrasonic imaging[69-71] has been corroborated by analytical and finite-element analysis modeling of coupled stress, gas diffusion, and oxidation theories.[72]

To illustrate the influence of local stress levels on interphase oxidation, Figure 7 shows the ultrasonic image of a unidirectional titanium matrix composite with circular notch configuration, made by the same constituents as the composite shown in Figure 6.[69] The sample was subjected to isothermal fatigue at elevated temperature (similar testing conditions as in the example shown in Figure 6). Four cracks at 45° angles to the fiber direction were developed from the hole; two of them became predominant and led to catastrophic failure. It was observed that the extent of oxidation along the fibers is maximum when the fibers are subjected to tensile stresses (arrow C in Figure 7). Also compressive stresses (arrow B in Figure 7) facilitate interphase oxidation compared to zero stress areas (between compressive B and tensile C stresses). The interphasial oxidation behavior observed in Figure 7 (zero degree unidirectional composite) is different from that shown in Figure 6 ([0/90]8 cross-ply configuration), which illustrates the effect of stresses imposed by the 90° fibers.[72]

Finally the role of various parameters such as local stress, temperature, and duration of exposure on the oxidation behavior of the interphase is illustrated in Figure 8, which also appears on the cover of this issue of *MRS Bulletin*.[70] Figure 8 shows the ultrasonic image of a unidirectional titanium matrix composite (same material and fiber layout as the composite shown in Figure 7) with a single-notch configuration subjected to out-of-phase thermomechanical fatigue for a long time (36 days).

References

1. R.C. Truell, C. Elbaum, and B.B. Chick, in *Ultrasonic Methods in Solid State Physics* (Academic Press, New York, 1969).
2. B.A. Auld, in *Acoustic Fields and Waves in Solids*, vols. I and II (J. Wiley and Sons, New York, 1973).
3. I.A. Viktorov, in *Rayleigh and Lamb Waves* (Plenum Press, New York, 1967).
4. D.R. Snider, H.P. Fredricksen, and S.C. Schneider, *J. Appl. Phys.* 52 (1981) p. 3215.
5. I. Feng, M. Tachiki, C. Krischer, and M. Levy, *ibid.* 53 (1982) p. 177.
6. E. Harnik and E. Sadar, *ibid.* 52 (1981) p. 3705.
7. G. Gorodetsky and I. Lachterman, *Rev. Sci. Instrum.* 82 (1981) p. 1386.
8. H.M. Ledbetter and J.G. Moulder, *J. Acous. Soc. Am.* 65 (1979) p. p. 840.
9. R.E. Lee and R.M. White, *J. Appl. Phys.* 12 (1968) p. 12.
10. P. Cielo, *Int. Adv. NDT* 11 (1985) p. 175
11. J.A. Cooper, R.A. Crosbie, R.J. McKie, and S.B. Palmer, *Proc. Ultrason. Int. 85* E25 (1985) p. 207.
12. D. Schneider, H.J. Schneider, and T. Schwarz, *Int. J. Sci. Technol. Diamond Related Mater.* (1992).
13. S.I. Rokhlin, Z. Ronen, and M.P. Dariel, *Thin Solid Films* 89 (1982) p. 109.
14. W.G.N. Neubauer, in *Physical Acoustic*, vol. 10, edited by W.P. Mason and R.N. Thurston (Academic Press, New York, 1973) p. 61.
15. D.E. Chimenti, A.F. Nayfeh, and D.L. Buter, *J. Appl. Phys.* 53 (1982) p. 170.
16. M. Hefets and S.I. Rokhlin, *J. Am. Ceram. Soc.* 75 (1992) p. 1839.
17. J.D. Achenbach, J.O. Kim, and Y.C. Lee, in *Advances in Acoustic Microscopy*, vol. 1, edited by A. Briggs (Plenum Press, New York, 1995).
18. R.S. Gilmore, K.C. Tam, J.D. Yong, and D.R. Howard, *Philos. Trans. R. Soc. London* A320 (1986) p. 215.
19. J. Johnson, R.B. Thompson, and E.E. Jamieson, in *Review of Progress in QNDE*, 14B, edited by D.O. Thompson and D.E. Chimenti (Plenum Press, New York, 1995) p. 1805.
20. D.A. Lee and D.M. Corbly, *IEEE Trans. Sonics Ultrason. Ind. Eng. Chem.* (1977) p. 206.
21. R.O. Claus and C.H. Palmer, *Appl. Phys. Lett.* 31 (1977) p. 547.
22. V. Kumar and G.S. Murty, *IEEE Trans. Sonic Ultrason. Ind. Eng. Chem.* (1982) p. 138.
23. G.S. Murty, *Phys. Earth Plant. Interiors* 11 (1975) p. 65.
24. S.I. Rokhlin, M. Hefets, and M. Rosen, *J. Appl. Phys.* 51 (1980) p. 3579.
25. *Ibid.* 52 (1981) p. 2847.

26. P.B. Nagy and L. Adler, in *Elastic Waves and Ultrasonic Nondestructive Evaluation*, edited by S.K. Datta, J.D. Achenbach, and Y.S. Rajapakse (North Holland, Amsterdam, 1990) p. 229.
27. W. Huang and S.I. Rokhlin, *Geophys. J. Int.* 118 (1994) p. 285.
28. J.M. Baik and R.B. Thompson, *J. Nondestr. Eval.* 4 (1984) p. 177.
29. F.J. Margetan, R.B. Thompson, J.H. Rose, and T.A. Gray, *ibid.* 11 (1992) p. 109.
30. S.I. Rokhlin and Y.J. Wang, in *Rev. Prog. QNDE* 10A (1991) p. 185.
31. J.D. Achenbach and M.J. Kitahara, *Acous. Soc. Am.* 80 (1986) p. 1209.
32. W. Huang and S.I. Rokhlin, *J. Nondestr. Eval.* 11 (1992) p. 185.
33. S.I. Rokhlin and Y.J. Wang, *J. Acoust. Soc. Am.* 89 (1991) p. 503.
34. S.I. Rokhlin and W. Huang, *ibid.* 94 (1993) p. 3405.
35. J.H. Rose, in *Rev. Prog. QNDE* 8B (1989) p. 1925.
36. J.H. Rose, R.A. Roberts, and F.J. Margetan, *Nondestr. Eval.* 11 (1992) p. 151.
37. P.B. Nagy and L. Adler, in *Rev. Prog. QNDE* 10A (1991) p. 177.
38. P.B. Nagy, *J. Nondestr. Eval.* 11 (1992) p. 127.
39. I. Yalda-Mooshabad, F.J. Margetan, T.A. Gray, and R.B. Thompson, *J. Nondestr. Eval.* 11 (1992) p. 141.
40. M. Kachanov, *Appl. Mech. Rev.* 45 (1992) p. 304.
41. Y.C. Chu and S.I. Rokhlin, in *Rev. Prog. QNDE* 12B (1993) p. 1475.
42. S.I. Rokhlin, Y.C. Chu, and W. Huang, in *Symposium on Wave Propagation and Emerging Technologies*, vol. 188, edited by V.K. Kinra, R.J. Clifton, and G.C. Johnson (ASME, 1994) p. 29.
43. W. Huang, S. Brisuda, and S.I. Rokhlin, *J. Acous. Soc. Am.* 97 (1995) p. 807.
44. Y.C. Chu and S.I. Rokhlin, *ibid.* 92 (1992) p. 920.
45. *Ibid.*, in *Ultrasonic Characterization and Mechanics of Interfaces*, vol. 117, edited by S.I. Rokhlin, S.K. Datta, and Y.D.S. Rajapakse (ASME AMD, 1993) p. 113.
46. W. Huang, S.I. Rokhlin, and Y.J. Wang, *Ultrasonics* 33 (5) (1995) p. 365.
47. T.E. Matikas and P. Karpur, *J. Appl. Phys.* 74 (1993) p. 228.
48. *Ibid.*, in *19th Review of Progress in QNDE*, vol. 12B, edited by D.O. Thompson and D.E. Chimenti (Plenum Press, New York, 1992) p. 1515.
49. S. Krishnamurthy, T.E. Matikas, P. Karpur, and D.B. Miracle, *Comps. Sci. Technol.* 54 (2) (1995) p. 161.
50. T.E. Matikas, P. Karpur, S. Krishnamurthy, and R.E. Dutton, *Appl. Comp. Mater.* 2 (1995) p. 293.
51. S. Krishnamurthy, T.E. Matikas, P. Karpur, and D.B. Miracle, *J. Mater. Res.* in press.
52. M.C. Waterbury, P. Karpur, T.E. Matikas, S. Krishnamurthy, and D.B. Miracle, *Comps. Sci. Technol.* 52 (2) (1994) p. 261.
53. T.E. Matikas, P. Karpur, R.E. Dutton, and R. Kim, *Mater. Eval.* 53 (9) (1995) p. 1045.
54. L.L. Shaw, T.E. Matikas, Prasanna Karpur, S. Hu, and D.B. Miracle, *Composites Part B: Engineering* in press.
55. S.I. Rokhlin, W. Huang, and Y.C. Chu, *Ultrasonics* 33 (5) (1995) p. 350.
56. S.I. Rokhlin, Y.C. Chu, and W. Huang, *Mech. Mater.* 21 (4) (1995) p. 251.
57. M. Gosz and J.D. Achenbach, in *Ultrasonic Characterization and Mechanics of Interfaces*, vol. 177, edited by S.I. Rokhlin, S.K. Datta, and Y.D.S. Rajapakse (ASME AMD, 1993) p. 125.
58. Y.C. Chu and S.I. Rokhlin, *J. Appl. Phys.* 76 (1994) p. 4121.
59. *Ibid., Mech. Mater.* 21 (3) (1995) p. 191.
60. *Ibid., Metall. Trans.* 27 (1) (1996) p. 165.
61. S.I. Rokhlin and W. Wang, *J. Acous. Soc. Am.* 91 (1992) p. 3303.
62. Y.C. Chu and S.I. Rokhlin, *ibid.* 95 (1994) p. 213.
63. Y.C. Chu, A.D. Degtyar, and S.I. Rokhlin, *ibid.* 95 (1994) p. 3191.
64. Y.C. Chu and S.I. Rokhlin, *ibid.* p. 3204.
65. R.T. Bhatt, NASA TM-102360 (1989).
66. Y.C. Chu, S.I. Rokhlin, and G.Y. Baaklini, *J. Eng. Mater. Technol.* 115 (1993) p. 237.
67. Y.C. Chu, A.I. Lavrentyev, S.I. Rokhlin, G.Y. Baaklini, and R.T. Bhatt, *J. Am. Ceram. Soc.* 78 (1995) p. 1809.
68. A.I. Lavrentyev and S.I. Rokhlin, *J. Appl. Phys.* 76 (8) (1994) p. 4643.
69. P. Karpur, T.E. Matikas, M.P. Blodgett, J.R. Jira, and D. Blatt, in *Special Applications and Advanced Techniques for Crack Size Determination*, ASTM STP 1251, edited by J.J. Ruschau and J.K. Donald (American Society for Testing and Materials, Philadelphia, 1995) p. 130.
70. D. Blatt, P. Karpur, D.A. Stubbs, and T.E. Matikas, *Scripta Metall. Mater.* 29 (1993) p. 851.
71. D. Blatt, P. Karpur, T.E. Matikas, M.P. Blodgett, and D.A. Stubbs, in *American Society for Composites 8th Technical Conference on Composite Materials* (Technomic Publishers, Cleveland, 1993) p. 531.
72. S. Hu, P. Karpur, and T.E. Matikas, in *21th Annual Review of Progress in QNDE*, 14B, edited by D.O. Thompson and D.E. Chimenti (Plenum Press, New York, 1995) p. 1263. □